Glucose biosensor based on functionalized ZnO nanowire/graphite films dispersed on a Pt electrode

2016 Nanotechnology 27 425501

(http://iopscience.iop.org/0957-4484/27/42/425501)

IOP Publishing Nanotechnology
Nanotechnology 27 (2016) 425501 (8pp) doi:10.1088/0957-4484/27/42/425501

Glucose biosensor based on functionalized ZnO nanowire/graphite films dispersed on a Pt electrode

P Gallay[1,2], E Tosi[1,2], R Madrid[3], M Tirado[2,4] and D Comedi[1,2]

[1] NanoProject and Laboratorio de Física del Sólido, Dep. Fisica, Facultad de Ciencias Exactas y Tecnología, Universidad Nacional de Tucumán, Av. Independencia 1800, 4000 San Miguel de Tucumán, Argentina
[2] Consejo Nacional de Investigaciones Científicas y Técnicas, CONICET, Argentina
[3] Laboratorio de Medios e Interfaces, Dep. Bioingeniería, Facultad de Ciencias Exactas y Tecnología, Universidad Nacional de Tucumán, and Instituto Superior de Investigaciones Biológicas (INSIBIO-UNT-CONICET), Av. Independencia 1800, 4000 San Miguel de Tucumán, Argentina
[4] NanoProject and Laboratorio de Nanomateriales y Propiedades Dieléctricas, Dep. Física, Facultad de Ciencias Exactas y Tecnología, Universidad Nacional de Tucumán, Av. Independencia 1800, 4000 San Miguel de Tucumán, Argentina

E-mail: dcomedi@herrera.unt.edu.ar

Received 4 May 2016, revised 2 August 2016
Accepted for publication 19 August 2016
Published 13 September 2016

Abstract

We present a glucose biosensor based on ZnO nanowire self-sustained films grown on compacted graphite flakes by the vapor transport method. Nanowire/graphite films were fragmented in water, filtered to form a colloidal suspension, subsequently functionalized with glucose oxidase and finally transferred to a metal electrode (Pt). The obtained devices were evaluated using scanning electron microscopy, energy-dispersive x-ray spectroscopy, cyclic voltammetry and chronoamperometry. The electrochemical responses of the devices were determined in buffer solutions with successive glucose aggregates using a tripolar electrode system. The nanostructured biosensors showed excellent analytical performance, with linear response to glucose concentrations, high sensitivity of up to $\approx 17\ \mu A\ cm^{-2}\ mM^{-1}$ in the 0.03–1.52 mM glucose concentration range, relatively low Michaelis–Menten constant, excellent reproducibility and a fast response. The detection limits are more than an order of magnitude lower than those achievable in commercial biosensors for glucose control, which is promising for the development of glucose monitoring methods that do not require blood extraction from potentially diabetic patients. The strong detection enhancements provided by the functionalized nanostructures are much larger than the electrode surface-area increase and are discussed in terms of the physical and chemical mechanisms involved in the detection and transduction processes.

Keywords: zinc oxide nanowires, functionalization, glucose, biosensor, nanostructured electrode

(Some figures may appear in colour only in the online journal)

1. Introduction

In recent years, semiconductor nanostructures such as nanowires (NWs) have been increasingly employed in sensing devices due to their large specific surface area and novel charge transport properties. One of these important applications includes biosensors for glucose level detection in the human body. Chronic diseases such as diabetes mellitus, a disorder triggered when the body loses its ability to produce enough insulin or to use it effectively, may cause lethal complications in human health [1]. Hence, enormous budgets have been devoted towards the development of devices for

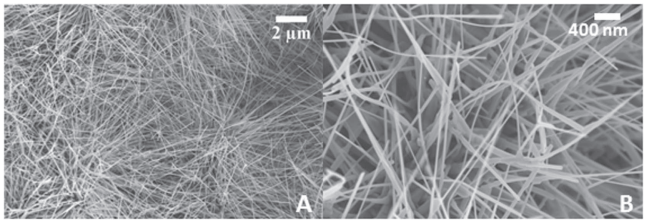

Figure 1. SEM images at two different magnifications of ZnO NWs grown on a compacted graphite substrate.

the early detection of anomalies in the glucose level in humans. Electrochemical biosensing strips capable of giving sufficiently reliable measures of glycaemia have been available in the market for many years. Nonetheless, sensitive devices capable of accurately and reproducibly determining low glucose concentration in real time in other body fluids besides blood, and as non-invasively as possible [2–5], are very desirable [6].

Different nanostructures have been explored to increase the sensitivity of electrochemical biosensors. NWs of ZnO [7, 8], a wide gap (3.37 eV) semiconductor often proposed for optoelectronic devices such as lasers, LEDs and solar cells, have been successfully tested. Given its biocompatibility, high isoelectric point ($IEP_{ZnO} \sim 9.5$), elevated surface activity, chemical stability and high electron communication feature, ZnO can be functionalized with a wide range of biological materials such as DNA, antibodies and enzymes [3, 9].

In this work, we describe a fabrication method for a glucose biosensor based on immobilization of glucose oxidase (GOx) enzyme on ZnO NWs grown from the vapor phase on compacted graphite flakes. The resulting device is characterized thoroughly and its glucose response is determined and compared with that corresponding to a non-nanostructured biosensor. The strong detection enhancement provided by the nanostructured biosensor is superior to the surface area enhancement and is therefore studied and discussed in terms of the physical and chemical mechanisms involved in the detection and transduction processes.

2. Experimental method

2.1. Growth of nanostructures

Self-sustained films of entangled ZnO NWs were grown on substrates of compacted graphite flakes using the vapor transport method. The Zn precursor vapor was produced through the carbothermal reduction of ZnO powder (99.99%) mixed with graphite flakes (99.9%) in an alumina crucible in the interior of a quartz tube connected to a vacuum and ultrapure (99.999%) Ar and O_2 gas feed systems. The ZnO + graphite crucible was heated from room temperature to 1050 °C under a steady Ar + O_2 (125 and 8 sccm, respectively) flow. The heating duration was established at 40 min by controlling the current in a resistive tubular furnace, and the temperature was then kept constant at this setpoint for 30 more minutes. At the end of this cycle, the gas flow, pump and heat current were simultaneously interrupted and the whole system allowed to cool down to room temperature prior to exposure of the final products to atmosphere.

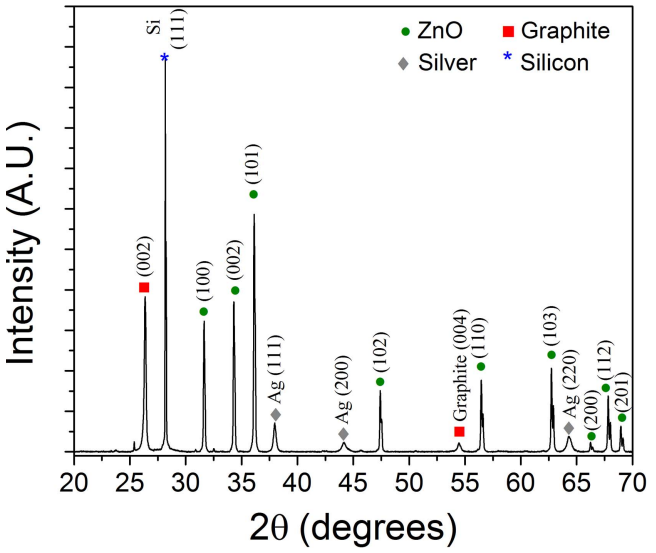

Figure 2. X-ray diffraction pattern obtained from a ZnO NW/graphite film attached onto a (111) oriented Si wafer with Ag paint.

During the thermal cycle, compacted graphite substrates were placed 26 cm downstream from the ZnO + graphite source. At this position the maximum temperature was lower than in the source (900 °C), hence Zn precursor vapors supersaturation was promoted, followed by their condensation on the graphite substrate, their oxidation and subsequent ZnO growth. Unlike other substrates such as Si wafers, no metal catalysts are needed for ZnO NW growth on graphite, which follows a vapor-solid growth mechanism [10, 11]. The final product is a self-sustained film of entangled ZnO NWs whose mean diameter is 65 nm and their lengths range between 2 and 6 μm. Scanning electron microscopy (SEM) images of these films are shown in figures 1(A) and (B).

Figure 2 shows an x-ray diffraction (XRD) pattern from an as-grown ZnO NWs on compacted graphite film. Since the films are brittle, the samples for the XRD study were prepared by attaching the ZnO NW films to (111) oriented Si wafers by dropping Ag paint on their edges. Hence, peaks due to Ag and the (111) planes of Si are also seen in addition to the graphite (004) and various ZnO peaks in figure 2. The pattern from the ZnO NWs agrees well with that from a polycrystalline ZnO standard, stemming from the fact that the ZnO NWs are randomly oriented.

2.2. Characterization

SEM images and energy-dispersive x-ray spectroscopy (EDS) spectra were acquired using a field emission microscope (FE-SEM Σigma) equipped with an *in situ* x-ray detector. XRD patterns from the deposited films were obtained by using a Bruker D8 Advance diffractometer and a CuK_α radiation source ($\lambda = 1.5418$ Å). Electrochemical analysis was conducted using a tripolar electrode system, consisting of the

working electrode, a reference Ag/AgCl (ER) and an AISI 304 concave stainless steel counter electrodes, within a cell provided with bubbling air. All electrochemical measurements were performed at room temperature using a Solartron 12 508 W frequency response analyzer with a Solartron 1287 electrochemical interface.

2.3. Sensor fabrication

The self-sustained ZnO NW film on graphite was introduced into distilled water in a 30 mg ml^{-1} proportion, agitated manually and then left to decant for 24 h. This final step aims at separating heavy film fragments from the smaller ones (which typically range between ≈1 μm and about 50 μm) that remain as dispersed microparticles in the supernatant colloid.

To functionalize the ZnO NWs, 190 μl of the supernatant colloid was mixed with 10 μl of a 43.4 mg ml^{-1} type VII glucose oxidase (GOx) [12] (from *Aspergillus niger*) solution in equimolar phosphate (PBS) buffer solution to generate a hydrophilic surface. PBS (0.01 M) was prepared from KH_2PO_4 and Na_2HPO_4 with 0.1 M KCl as supporting electrolyte. After stirring, the solution was allowed to rest for 24 h in a refrigerator to enable the formation of [NWs–GOx] complexes.

Subsequently, 80 μl of this solution was transferred to a previously polished Pt electrode with, sequentially, 1.0, 0.3 and 0.05 μm alumina powders. The Pt electrode area was 1.76 cm^2. A SEM image at low magnification of the result of this procedure is shown in figure 3(A). The deposited functionalized film fragments have sizes varying mostly between 20 and 40 μm. From the size distribution, shown in the histogram of figure 3(B), we estimate that, following this drop coating procedure, a ∼20% of the Pt electrode is covered with the functionalized ZnO NW/graphite fragments. After 24 h, 80 μl of commercial polymeric Nafion® resin 0.5 P/P (Nf) was dropped on top of the biosensor and left to dry for 24 h. This step is essential to preserve the biosensor electrode integrity during electrochemical testing and enhances the anti-interference ability of the biosensor.

Various control electrodes were also prepared by depositing identical quantities of Nf directly on the polished Pt or on non-functionalized ZnO NW modified Pt electrode. All chemicals were purchased from Sigma-Aldrich.

3. Results

Figure 4 shows high magnification SEM images of some ZnO NWs-on-graphite film fragments that were extracted from their liquid dispersion. Figures 4(A), (B) correspond to bare NWs, while figures 4(C) and (D) are NWs after functionalization with the GOx enzyme. Since it is an organic material, the GOx formations on the NWs are not readily seen by electron microscopy. However, indirect information can be extracted from the NW diameters, as shown in the histograms depicted in figure 4(E). From the shift of the NW mean diameter from 65 nm (bare NWs) to 85 nm (functionalized

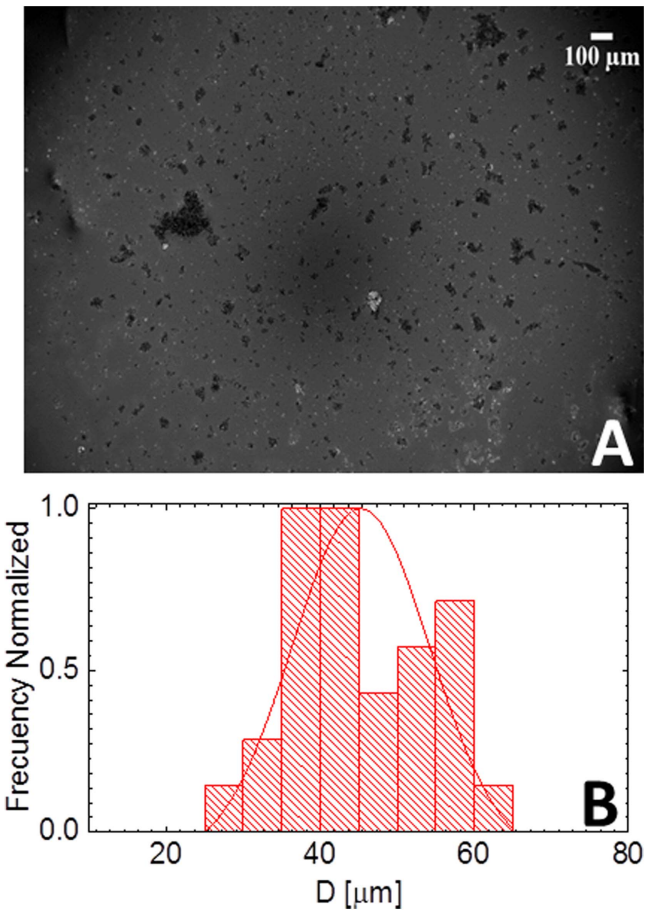

Figure 3. (A) SEM image showing the resulting overall coverage of the Pt electrode after the deposition of the ZnO NW/graphite film fragments. (B) Histogram of approximate fragment sizes.

NWs), it can be concluded that the GOx is deposited on the NWs as a conformal film approximately 10 nm thick.

It is clear from the comparison of figures 1 and 4 that most of the NWs are cut during the transfer from the growth film (where their lengths are 2–6 μm) to the Pt electrode (where they are typically shorter than 2 μm length). However, it should be noted that this does not severely affect the final area-to-volume ratios of the NWs, as they are mainly determined by the NWs radii rather than by their lengths.

The compositional distribution over some of the transferred functionalized ZnO NW/graphite particles was determined by acquiring EDS maps on samples produced by depositing a drop sample of the supernatant colloid on a Au covered Si wafer and evaporating the liquid solvent by mild heating (see figures 5(A)–(D)). As can be seen, the particles contain, as expected, mainly C (from the graphite substrate), and Zn and O from the ZnO NWs. The spatial coincidence between Zn and O, whose distributions notably differ from that of C, shows that these signals come from ZnO NW formations that grew on the graphite substrate, covering most of it. As shown in the full EDS spectrum (figure 5(E)), other elements are also detected, such as Cl and K, which originate from the buffer solution used for the NW transfer and functionalization. Also seen is Au, which comes from the thin Au

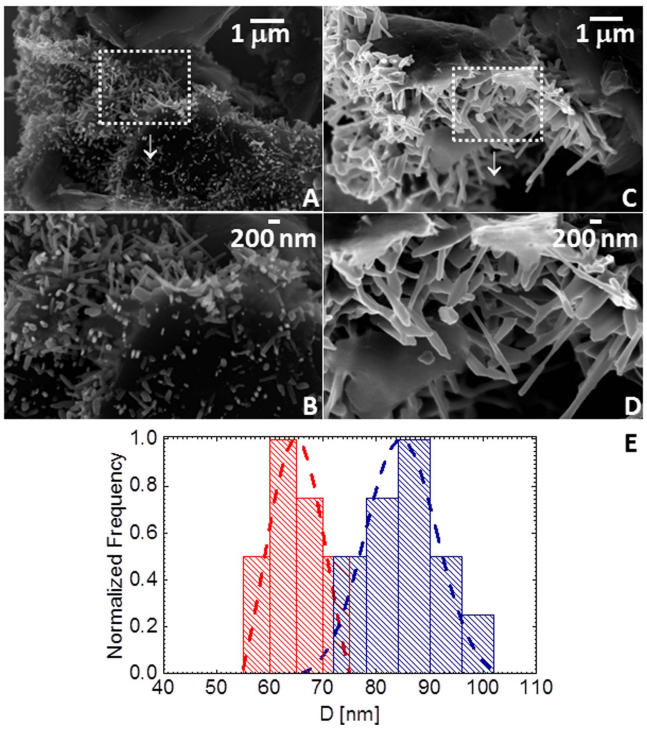

Figure 4. SEM images of ZnO NWs/graphite particles extracted from the liquid dispersion before (A), (B) and after (C), (D) functionalization with GOx. (E) shows NW diameter histograms and corresponding Gaussian fits as obtained from SEM images of bare (red on the left) and functionalized (blue on the right) ZnO NWs.

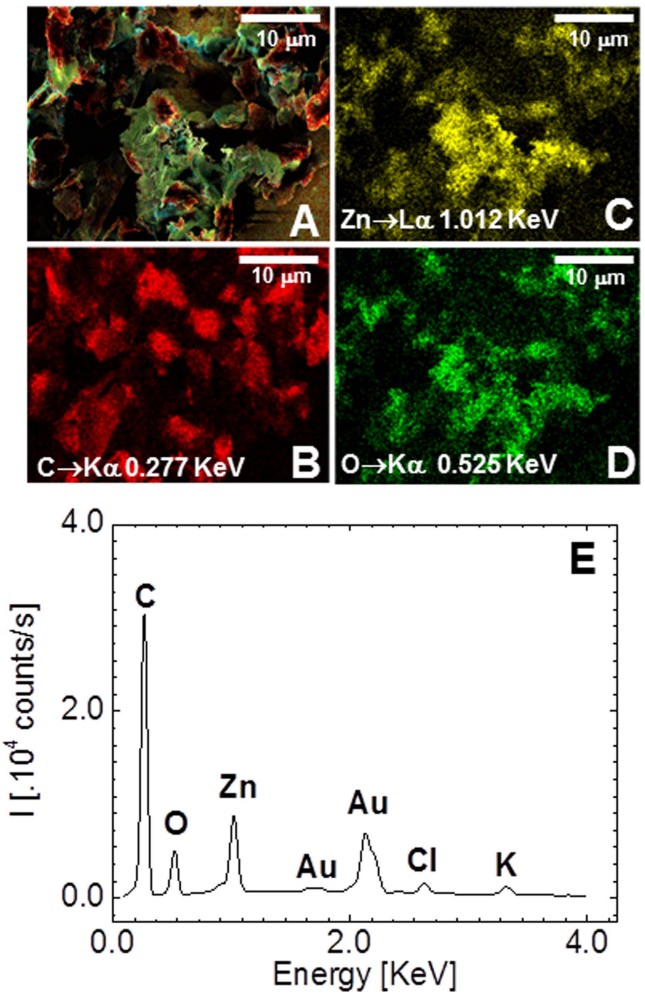

Figure 5. (A) EDS maps of all detected elements together, and individual EDS maps for (B) carbon, (C) zinc and (D) oxygen, acquired on some of the particles found in a drop sample of the supernatant colloid. (E) EDS spectrum from the whole region.

layer that was sputter deposited on these samples to avoid their charging by continuous electron bombardment during the analysis.

In figure 6, cyclic voltammograms (CV) obtained for different electrode configurations are shown. Figure 6(A) depicts a CV for Pt/Nf and Pt/NWs/Nf electrodes in 0.01 M PBS buffer for a large potential scan interval (from −0.95 to +0.95 V). The observed curves establish the response of the basic biosensor components Pt/Nf and Pt/NWs/Nf in buffer solution and also demonstrate the absence of electroactive interfering species in the PBS buffer solution.

Figure 6(B) shows CVs measured for the ZnO NW biosensor in PBS with and without glucose. Nearly at 600 mV a current increase is detected exhibiting a peak maximum above 800 mV when glucose is present. This peak corresponds to the oxidation of hydrogen peroxide (H_2O_2) that is produced following the prior oxidation of glucose catalyzed by the functionalizing enzyme (GOx).

Figure 7(A) shows the time evolution of the amperometric response of the biosensor device after a potential of 900 mV is applied at $t = 0$ and after multiple aggregates of 0.14 mM glucose each are added to the buffer solution. The first part of the curve shows how the system approaches a steady state after the potential is applied and then it responds promptly to the successive glucose aggregates. The amperometric response of the NW biosensor is compared with that of a functionalized Pt electrode without the presence of NWs in figure 7(B). The much more rapid and sensitive response of the nanostructured electrode is evident. The signal-to-noise ratio (SNR) for the sensor with NWs is ∼13.4 while for the sensor without nanostructures is initially ∼1.5, however, as seen in figure 7(B), it rapidly degrades with time and with further glucose aggregates until the SNR becomes very large so the glucose becomes virtually undetectable. This problem is solved completely in the nanostructured biosensor.

4. Discussion

The glucose in GOx functionalized electrodes is detected via the following electrochemical reactions [13]:

$$\beta\text{-D-Glucose}_{(aq)} \xrightarrow{\text{GOx}} \text{D-Glucono-1,5 lactone}_{(aq)}, \quad (1)$$

$$O_{2(aq)} \xrightarrow{\text{GOx} - \text{FADH}_2 \rightleftharpoons \text{GOx} - \text{FAD}} H_2O_{2(aq)}, \quad (2)$$

$$H_2O_{2(aq)} \xrightarrow{900\,\text{mV}} \uparrow O_{2(g)} + 2H^+_{(aq)} + 2e^-. \quad (3)$$

Initially, the GOx enzyme oxidizes the glucose (equation (1)), while using O_2 from water as cofactor to oxidize the flavin

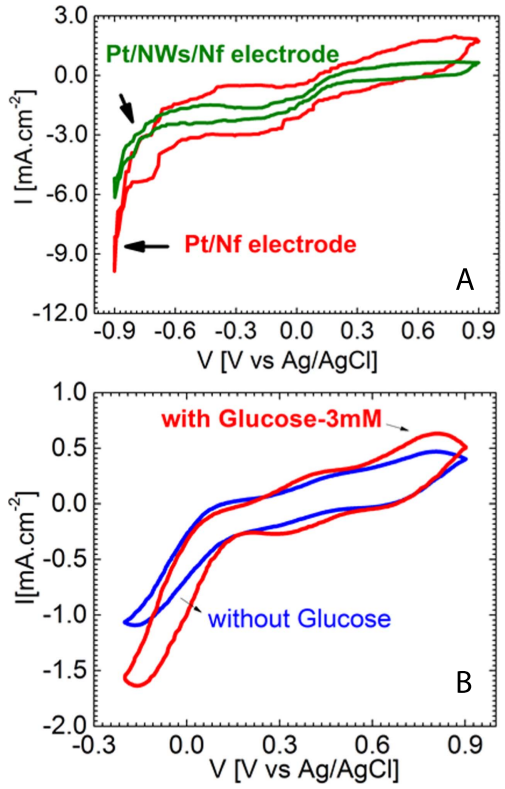

Figure 6. (red) Cyclic voltammograms for (A) Pt/NWs/Nf (green) and Pt/Nf (red) electrodes in 0.01 M PBS buffer (pH 7.4) with a potential scan rate of 50 mV s^{-1}; and for (B) a glucose biosensor with a potential scan rate of 50 mV s^{-1} in 0.01 M PBS (pH 7.4) buffer without (blue) and with 3 mM glucose (red).

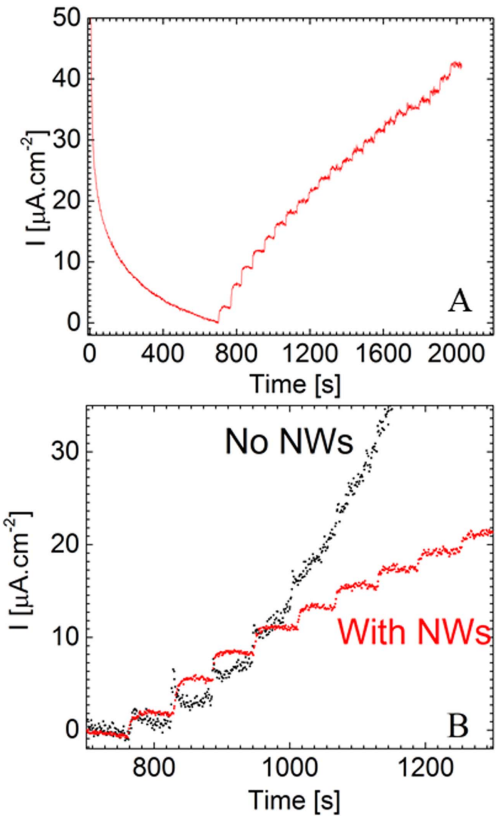

Figure 7. (A) Amperometric glucose response of the biosensor (current density as a function of time) in buffer to multiple 0.14 mM glucose aggregates, pH 7.4, with stirring. (B) Comparison of responses between sensors with and without NWs as a function of time for multiple 0.14 mM glucose aggregates.

adenine dinucleotide group, resulting in the production of H_2O_2 (equation (2)). Both processes are enabled by GOx enzyme catalysis. The oxidation of H_2O_2 (equation (3)), in turn, is commonly used to evaluate the amperometric response of the glucose biosensor.

As in previous reports, one is tempted to attribute the detection enhancements provided by the ZnO nanostructures to a surface area increase of the working electrode. However, we estimate that the increase of electrode surface area for the present NW morphology and Pt electrode coverage amounts to less than a factor of two. Hence, while this is certainly a partial cause, it is clear that the improvements provided by the ZnO nanostructures, which amount to increases by an initial factor of ~ten in the SNR ratio and quickly become orders of magnitude larger for successive glucose aggregates (figure 5(B)), must be mainly due to an enhanced activity of the reactions listed in equations (1)–(3) provided by the ZnO–GOx complexes. The formation of ZnO–GOx complexes during functionalization is facilitated by the high isoelectric point value of ZnO, which allows the efficient immobilization of high concentrations of acidic enzymes by electrostatic interactions with high binding stability. It is known that GOx molecules are negatively charged in neutral pH solutions (as the one used here for NW functionalization) and hence they are readily attracted, adsorbed and immobilized onto the positively charged ZnO NWs. The ZnO biocompatibility provides also a favorable microenvironment for retaining enzyme activity.

Other question that should be considered is the specific electrochemical catalytic action of these complexes, which are related to their intrinsic chemical and stereochemical properties. For instance, it has been shown that defects on ZnO surfaces may act as highly efficient redox sites [14]. However, other factors associated with morphology related transport enhancement phenomena at the electrolyte/electrode interface may play a role. One of these would involve effects from local electric field gradients produced by the sharp NW morphology. The highly divergent electric field expected near NW tips should produce a force on the glucose polar molecules that could preferentially guide them towards the functionalized ZnO NWs.

In order to gain further insight into the detection enhancement effects provided by the nanostructures on the Pt electrode, we have also evaluated the biosensors by amperometrically detecting the reduction and oxidation reactions of the reference $Fe(CN)_6^{-4}/Fe(CN)_6^{-3}$ redox couple. The corresponding CVs are shown in figure 8. Again, the measured current is seen to be much larger for the nanostructured biosensor than for the Pt electrode without NWs. If electron transfer at the electrode has no diffusive components, the peak

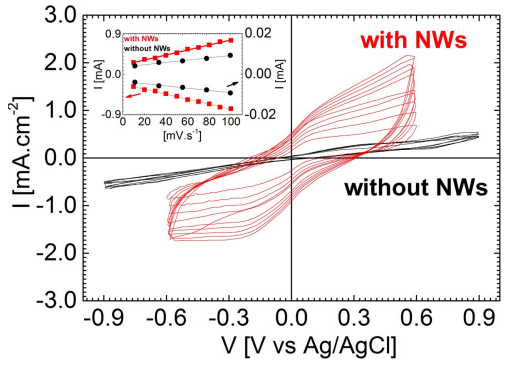

Figure 8. Amperometric response to the $Fe(CN)_6^{-4}/Fe(CN)_6^{-3}$ redox couple of GOx functionalized biosensors with (red) and without (black) NWs for different scan rates. Insert: cathodic and anodic peak currents I_{pc} y I_{ac}, for both sensors, as functions of the scan rate. Note the very different scales.

Table 1. Density of electroactive sites on biosensor electrodes as determined from data in figure 8 and using equation (4).

	Γ^* (moles cm^{-2})
No NWs	1.5×10^{-13}
With NWs	5.8×10^{-12}

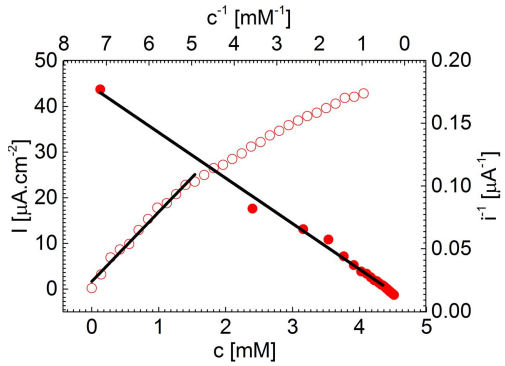

Figure 9. Open symbols: calibration curve (current density as a function of the glucose concentration) for the biosensor with NWs. The linear response for low glucose concentrations is indicated. Closed symbols: corresponding Lineweaver–Burk plot (reciprocal current as a function of the reciprocal glucose concentration); the linear behavior in the whole glucose concentration range is evident.

current (i_p) is given by equation (4) [15, 16],

$$i_p = n^2F^2\nu A\Gamma^*/4RT, \quad (4)$$

where n is the number of exchanged electrons, F is the Faraday constant, ν is the scan velocity, and A is the active area of the electrode. Using equation (4), one can estimate an average density per unit area of electroactive sites on the working electrode surface, Γ^*, by, for instance, measuring i_p as a function of ν. This can be done in this case for both, the anodic and cathodic peaks (i_{pa} and i_{pc}) on the voltammograms, as shown in the insert of figure 8. The accurate linearity of the data confirms the applicability of equation (4) to the present experiment.

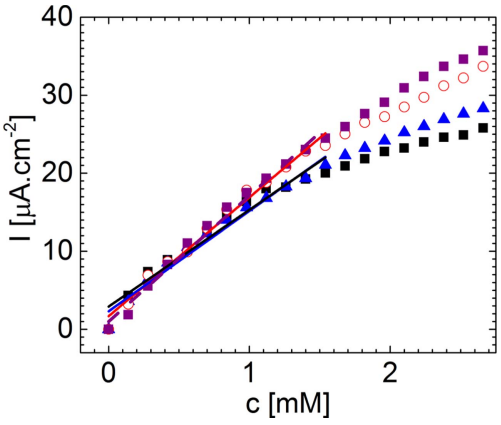

Figure 10. Degree of reproducibility of biosensor electrodes as examined by comparing various independently determined calibration curves.

Table 1 shows the results obtained from this analysis. As seen, Γ^* is larger by a factor of ~40 in the nanostructured biosensor. Despite the semiconducting characteristics of the ZnO NWs, they respond sensitively to the reduction and oxidation charge transfer processes. The value of 5.8×10^{-12} mol cm^{-2} (table 1) is comparable to, and falls between, those reported for C nanotubes [17] and Au nanoparticle [18] modified GOx functionalized electrodes.

We note in passing that the $Fe(CN)_6^{-4}/Fe(CN)_6^{-3}$ couple redox peaks in figure 8 are shifted toward lower potentials for the nanostructured biosensor as compared to the electrode without NWs. This supports the idea of the presence of highly efficient electroactive sites on the ZnO NW surfaces or on the (ZnO–GOx) complexes. Furthermore, as mentioned before, the three dimensional character of the nanostructured electrode implies in additional transport mechanisms of the electroactive species that should enhance the electron communication and detection capabilities of the NW modified against the non-nanostructured electrode. In this context, it is interesting to note that similar behaviors have been observed in other nanostructured systems, such as porous graphene electrodes [19], where effective electrocatalytic effects were demonstrated to be due to a beneficial diffusive coupling between the electrode and the electrolyte, which becomes more pronounced with increasing electrode porosity.

Next, we determine the overall glucose detection performance of the nanostructured biosensor by plotting, in figure 9, the calibration curve obtained directly from the amperometric data in figure 7. The dynamic range for this calibration is 0.03–1.52 mM. The biosensor sensitivity obtained from the linear fit to the low concentration range of the experimental curve is 17 μA cm^{-2} mM^{-1} ($R^2 = 0.983$).

The detection limit (LOD), in turn, is ~9 μM while the limit of quantification (LOQ) is ~30 μM. To evaluate the catalytic performance of the enzyme, we determine the Michaelis–Menten constant (K_m), which is usually defined as the substrate concentration at which the enzymatic reaction rate reaches a value equal to half its maximum. In our case, however, since the enzyme is immobilized over the ZnO nanostructures, the value obtained is for the [ZnO–GOx]

Table 2. Range of sensitivity and LOD values determined for the biosensors developed in the present work and from previous reports on ZnO NW-based glucose biosensors from the literature.

System	Sensitivity (μA mM^{-1}cm^{-2})	LOD (μM)	Reference
GOx/ZnO-NWs/graphite	13–17	3–13	This work
GOx/ZnO-NWs	15.33	20	[20]
GOx/ZnO-NWs	19.5	<50	[21]
Linker mediated GOx/ZnO NWs	6.07–17.72	0.02	[24]
GOx/ZnO-NWs/paper	8.24	59.5	[25]

complexes. Hence, an apparent constant, K_m^{app}, can be obtained from the Lineweaver–Burk plot described by the equation:

$$\frac{1}{i} = \frac{K_m^{app}}{i_{max}}\frac{1}{c} + \frac{1}{i_{max}}, \quad (5)$$

where i is the measured current, c is the glucose concentration, and i_{max} is a maximum current obtained by extrapolating $1/i$ to its value for $1/c = 0$. The Lineweaver–Burk plot is shown as red dot symbols in figure 7. The value found is $K_m^{app} = 2.11$ mM, which compares well to those reported in the literature for other ZnO NW modified sensors [20, 21]. As it has been noted previously, this value is significantly lower than those obtained when other nanomaterials, such as Au nanoparticles or nanoporous TiO_2 films, are used [22, 23]. This further demonstrates the excellent beneficial support characteristics of ZnO for GOx and probably for other biological materials as well.

Finally, the reproducibility of the biosensor electrodes is examined in figure 10. As can be seen, there is some dispersion, especially in the saturation region. The sensitivity reproducibility amounts to 10% (standard deviation) in the 0–1.52 mM concentration region. The range of sensitivity and LOD values deduced from these data are shown in table 2 and compared with some of those reported for other ZnO NW based biosensor devices [20–22, 24, 25]. As can be seen, our biosensors present sensitivities comparable to those fabricated by other methods. For the LOD values, in turn, the present method yields lower values than those reported for other electrostatically functionalized ZnO NW-based biosensors [20, 21, 25], showing its excellent performance. It should be noted, however, that a much lower LOD value has been reported for linker mediated GOx functionalized ZnO NWs [24]. Although the values obtained here readily match those needed for glucose monitoring in body fluids other than blood from potentially diabetic patients (such as ~170 μm in tear [26], for instance), the process of linker mediated GOx functionalization of NWs could be easily incorporated to our fabrication method for future applications where lower LOD values may be required.

5. Conclusions

In this work, the steps for the fabrication of a glucose biosensor based on ZnO NWs deposited on graphite flakes by vapor-transport without metal catalyst are described. It is shown that the obtained biosensor is capable of reliably and reproducibly detecting very low glucose concentrations (LOD ~ 9 μM, LOQ ~ 30 μM), suggesting its applicability for the non-invasive control of diabetes in body fluids other than blood [6]. The analysis of the nanostructured system shows detection improvements by several orders of magnitude with respect to the non-nanostructured biosensor. Analytical parameters for the ZnO NW modified electrode samples emphasize the excellent properties of ZnO to immobilize glucose oxidase and to form a biospecific interface, with good sensitivity, relatively low LODs, fast response and good reproducibility for the detection of D (+) − glucose. The method developed here for growth of ZnO NWs on graphite, their functionalization and transfer to useful low impedance electrodes can be further optimized. However, it is highly versatile in its present form and should be easily extended to other enzymes and materials for biorecognition.

Acknowledgments

This work was partially funded by the Argentinean agencies CONICET, ANPCyT-FONCyT (PICT2010-0400), Fundación Argentina de Nanotecnología (FAN, Proyecto Presemilla) and PIUNT 26/E535. The authors thank the Laboratory of Electron Microscopy and X-Ray Analysis (LAMARX-UNC) for SEM images and EDS maps.

References

[1] International Diabetes Federation 2015 *IDF Diabetes Atlas* 7th edn (Brussels: International Diabetes Federation) (http://diabetesatlas.org)

[2] Wang Y, Xu H, Zhang J and Li G 2008 Electrochemical sensors for clinic analysis *Sensors* **8** 2043–81

[3] Li X, Zhao C and Liu X 2015 A paper-based microfluidic biosensor integrating zinc oxide nanowires for electrochemical glucose detection *Microsyst. Nanoeng.* **1** 15014

[4] Zhao Y, Deng P, Nie Y, Wang P, Zhang Y, Xing L and Xue X 2014 Biomolecule-adsorption-dependent piezoelectric output of ZnO nanowire nanogenerator and its application as self-powered active biosensor *Biosensors Bioelectron.* **57** 269–75

[5] Xue X, Qu Z, Fu Y, Yu B, Xing L and Zhang Y 2016 Self-powered electronic-skin for detecting glucose level in body fluid basing on piezo-enzymatic-reaction coupling process *Nano Energy* **26** 148–56

[6] Lee H *et al* 2016 A graphene-based electrochemical device with thermoresponsive microneedles for diabetes monitoring and therapy *Nat. Nanotechnol.* **11** 566–72
[7] Wang Z L 2004 Zinc oxide nanostructures: growth, properties and applications *J. Phys. Condens. Matter* **16** R829
[8] Dasgupta N P, Sun J, Liu C, Brittman S, Andrews S C, Lim J, Gao H, Yan R and Yang R 2014 25th anniversary article: semiconductor nanowires—synthesis, characterization, and applications *Adv. Mater.* **26** 2137–84
[9] Yeom S H, Kang B H, Kim K J and Kang S W 2010 Nanostructures in biosensor-a review *Front. Biosci.* **16** 997–1023
[10] Vega N C, Wallar R, Caram J, Grinblat G, Tirado M, LaPierre R R and Comedi D 2012 ZnO nanowire co-growth on SiO_2 and C by carbothermal reduction and vapour advection *Nanotechnology* **23** 275602
[11] Comedi D, Tirado M, Zapata C, Heluani S P, Villafuerte M, Mohseni P K and LaPierre R R 2010 Randomly oriented ZnO nanowires grown on amorphous SiO_2 by metal-catalyzed vapour deposition *J. Alloys Compd.* **495** 439–42
[12] Bankar S B, Bule M V, Singhal R S and Ananthanarayan L 2009 Glucose oxidase-an overview *Biotechnol. Adv.* **27** 489–501
[13] Wilson R and Turner A P F 1992 Glucose oxidase: an ideal enzyme *Biosensors Bioelectron.* **7** 165–85
[14] Peyghan A A, Laeen S P, Aslanzadeh S A and Moradi M 2014 Hydrogen peroxide reduction in the oxygen vacancies of ZnO nanotubes *Thin Solid Films* **556** 566–70
[15] Ceroni P, Credi A and Venturi M (ed) 2010 *Electrochemistry of Functional Supramolecular Systems* (New York: Wiley) p 186
[16] Karuppiah C, Palanisamy S, Chen S M, Veeramani V and Periakaruppan P 2014 Direct electrochemistry of glucose oxidase and sensing glucose using a screen-printed carbon electrode modified with graphite nanosheets and zinc oxide nanoparticles *Microchim. Acta* **181** 1843–50
[17] Zhang J, Feng M and Tachikawa H 2007 Layer-by-layer fabrication and direct electrochemistry of glucose oxidase on single wall carbon nanotubes *Biosensors Bioelectron.* **22** 3036–41
[18] Liu S and Ju H 2003 Reagentless glucose biosensor based on direct electron transfer of glucose oxidase immobilized on colloidal gold modified carbon paste electrode *Biosensors Bioelectron.* **19** 177–83
[19] Punckt C, Pope M A and Aksay I A 2013 On the electrochemical response of porous functionalized graphene electrodes *J. Phys. Chem.* C **117** 16076–86
[20] Wang J X, Sun X W, Wei A, Lei Y, Cai X P, Li C M and Dong Z L 2006 Zinc oxide nanocomb biosensor for glucose detection *Appl. Phys. Lett.* **88** 3106
[21] Pradhan D, Niroui F and Leung K T 2010 High-performance, flexible enzymatic glucose biosensor based on ZnO nanowires supported on a gold-coated polyester substrate *ACS Appl. Mater. Interfaces* **2** 2409–12
[22] Rahman M M, Ahammad A J, Jin J H, Ahn S J and Lee J J 2010 A comprehensive review of glucose biosensors based on nanostructured metal-oxides *Sensors* **10** 4855–86
[23] Cao H, Zhu Y, Tang L, Yang X and Li C 2008 A glucose biosensor based on immobilization of glucose oxidase into 3D macroporous TiO_2 *Electroanalysis* **20** 2223–8
[24] Jung J and Lim S 2013 ZnO nanowire-based glucose biosensors with different coupling agents *Appl. Surf. Sci.* **265** 24–9
[25] Li X, Zhao C and Liu X 2015 A paper-based microfluidic biosensor integrating zinc oxide nanowires for electrochemical glucose detection *Microsyst. Nanoeng.* **1** 15014
[26] Zhang J, Hodge W, Hutnick C and Wang X 2011 Noninvasive diagnostic devices for diabetes through measuring tear glucose *J. Diabetes Sci. Technol.* **5** 166–72